International Journal of Research in Engineering, Science and Management
Volume-1, Issue-11, November-2018
www.ijresm.com | ISSN (Online): 2581-5792

A Study of Microstructure and Mechanical Property Relationship of TIG Welded P91316l Dissimilar Steel Joint

R. Raveen[1], R. Ajithraj Bhat[2], R. Balaji[3], K. Dinesh Choudhry[4]
[1]*Assistant Professor, Dept. of Mechanical Engg., Sri Ramakrishna Engineering College, Coimbatore, India*
[2]*Student, Dept. of Mechanical Engg., Sri Ramakrishna Engineering College, Coimbatore, India*

***Abstract*: The work explains the effect of activating flux tungsten inert gas (TIG) welding on the microstructural, mechanical and corrosion behaviour of the 316L stainless steel (SS) and P91 steel weldment. The current study also demonstrated the comprehensive structure– property relationships of dissimilar joint weldment using the collective techniques of optical macro and microscopy, electron microscopy, and Energy-dispersive X-ray spectroscopy (EDS) techniques. Microstructure study reveals the presence of austenite and martensite in different zones of the weldment. The Maximum impact energy was absorbed by the 316L SS side heat affected zone while minimum by P91 steel side HAZ during the Charpy toughness test.**

***Keywords*: TIG, Dissimilar joint, P91, 316L, Mechanical properties**

1. Introduction

Modified 9Cr1Mo (P91) martensitic steeland 316L austenitic stainless steel combination was frequently used in high performance power plants. Hence both materials possess admirable mechanical and corrosion properties at high temperature. The Trimetallic configuration joints are generally recommended for fabrication of the P91 with 316L, which is a quite complex and an expensive procedure.

Activating flux tungsten inert gas welding process is a novel approach to weld the thick gauge sections without filler material. In this process, a thin layer of activating flux is coated over the metal surface prior to welding. That 12 mm thick gauge sections can be easily welded using on TIG welding process in a single pass. The main reasons for the deep and narrow weld penetration during TIG welding. We used TIG process to weld 6 mm thick 316L and compared its properties with the multipass TIG weld of the same. The study claimed that TIG weldment possessed better mechanical properties weldment. Although there are sufficient numbers of literature are available on the TIG welding of P91 steel and 316L stainless steel separately. However, the dissimilar weld between P91 steel and 316L stainless steel using TIG welding process is not reported yet. Bimetallic butt joint between P91 steel and 316L SS could help to cut a major fraction of the fabrication cost and improve the productivity.

Dissimilar welding between P91 steel with 316L stainless steel by TIG welding process possesses a different kind of challenges due to the difference in material properties such as chemical composition, thermal and electrical conductivity, and coefficient of thermal expansion. The asymmetric weld bead is a major problem observed during single pass conventional welding as well as TIG welding of the dissimilar steels. In the current work, authors have reported the symmetric weld bead of the dissimilar weld joint between the P91 steel and 316L SS in a single pass by using TIG welding process. the effort has been also made to analyze the weld joint integrity through different characterizations processes such as macro and microstructure study, tensile test, Charpy toughness test .The current study aims to offer the guidance to the welding of the dissimilar steel joint between P91steel and 316L SS.

2. Materials and experimental procedure

Modified 9Cr1Mo ferritic (P91) and 316L austenitic stainless steels were selected as base metals for the current work. The chemical compositions of the as-received base metals were analyzed using optical emission spectrometer (OES) (Metalvision-1008i) and presented in Table 1. The microstructures of P91 and 316L were studied using an electron microscope. The prior austenite grain boundaries (PAGBs) were observed in the as-received P91 steel. Precipitates in different shapes and sizes were also noticed on the grain boundaries and within the grain matrix. X-ray spectroscopy (EDS) study. The EDS spectrum and the chemical composition of the precipitates are presented in. Elemental composition indicated the presence of M23C6 (M: Fe, Mo, Mn, and Cr) and MX (M: Nb, V, and X: C, N) type of precipitates.

P91 and 316L steel plates of size 150×65×8 mm^3 were prepared for the single pass butt weld joint. The plates were tacked at both the ends and then cleaned with abrasive paper. Multicomponent flux comprising 35 % TiO2, 40 % SiO2, 15 % NiO, and 10 % CuO was used as an activating flux. The activating flux was baked at 150 °C for about 2 hours for dehumidification if any, prior to mixing it in the solvent. Acetone was used as a solvent. A direct current electrode

International Journal of Research in Engineering, Science and Management
Volume-1, Issue-11, November-2018
www.ijresm.com | ISSN (Online): 2581-5792

Table 1
Chemical composition (Weight %) of as received base metals and weld metal

Elements	C	Si	Mn	Cr	Mo	Cu	Ti	V	N	Ni	Fe
P91 steel	0.09	0.31	0.43	8.17	0.81	0.13	0.01	0.26	0.04	0.43	Balanced
316L SS	0.04	0.40	1.37	18.67	0.23	0.30	-	-	-	8.25	

Table 2
Welding process parameters

Welding current	Welding voltage	Welding speed	Arc length	Shielding gas	Electrode tip angle (°)	Electrode diameter
230 A	14 V-16 V	80±2 mm/min	3 mm	Pure argon with 10 l/min	60±1.5	2.9 mm

Table 3
Elemental composition at different position in the weld fusion zone

Wt%	Cr	Si	Mo	V	Nb	W	Ni	Mn	C	N	Cu	Cr_{eq}	Ni_{eq}	FF
Area1	14.77	0.37	0.62	0.13	0.15	0.09	5.78	1.35	0.05	0.01	0.25	17.42	8.28	9.14
Area2	11.58	0.33	0.98	0.11	0.4	-	4.02	0.58	0.09	0.02	0.19	14.96	7.567	7.39

negative (DCEN) power source was used for TIG welding. A water cooled TIG torch consisting tungsten electrode of diameter 3 mm was mounted on the mechanized tractor to obtain constant welding speed. Welding process parameters used during the current work is elucidated in Table 2.

After welding the weld joint was first visually inspected to check the surface defects such as surface cracks, porosity, and incomplete fusion. The defect free weldment was then subjected to measure the angular distortion. The weldment was then cut into different sections from the transverse direction to carry out the metallurgical, mechanical, and corrosion behaviour study as shown in Fig. 1. Samples for metallurgical examination were prepared using standard metallographic procedures including grinding, mounting, polishing and etching.

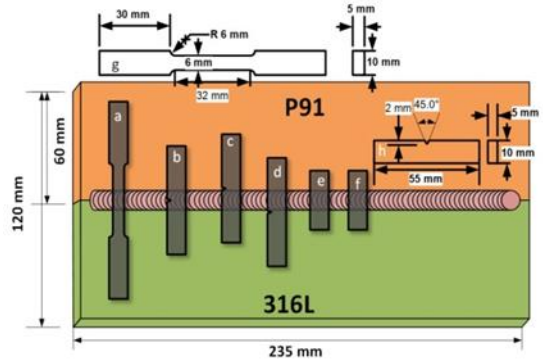

Fig. 1. Location of samples

The Fig. 1, Schematic represents the location from samples were taken for (a) tensile test, (b) Charpy toughness for weld fusion zone, (c) Charpy toughness for P91 side heat affected zone (HAZ), (d) Charpy toughness for 316L side HAZ, (e) metallographic and microhardness test, and (f) dimensional detail of the tensile and Charpy toughness test samples

The macroscopic study of the weldment was carried out using a stereo-microscope. Energy Dispersive X-ray analysis (EDS) and X-ray diffraction (XRD) were used to investigate the chemical composition and distribution of the elements.

The mechanical properties of the weldment were analyzed in terms of Vickers micro hardness, transverse tensile properties, and Charpy toughness. Vickers micro hardness measurements were carried out on the transverse cross-section specimen comprising all the zones of the weldment at a regular interval of 0.25 mm using the micro hardness tester. ASTM standard E92–16 was followed during the Vickers hardness measurement. To conduct the tensile test, standard sub-size tensile specimens were prepared according to ASTM E8M-04 with a gauge length, width, and thickness of 25 mm, 6 mm, and 5 mm, respectively. Room temperature tensile tests were performed on the Instron Vertical Tensile Testing machine (INSTRON 5980) at a crosshead speed of 1 mm/min. SubsizeCharpy toughness test samples, of size 55×10×5 mm^3 with 2 mm central V-shaped notch were prepared according to ASTM A370.

3. Result and Discussion

A. Visual inspection of the weldment

A welded plate is shown in the Fig. 2. The front and back side of the weldment suggests that weld was free from any surface discontinuity such as porosity and cracks. The back side of the weldment also suggests that penetration was through thickness all along the weld line without any discontinuity. The schematic of the process used for measuring the angular. During measurement, the dial gauge was moved along the x-axis from the weld center to the edge of the plate through a distance ΔX. Thereafter, a vertical displacement ΔZ was obtained from the dial gauge.

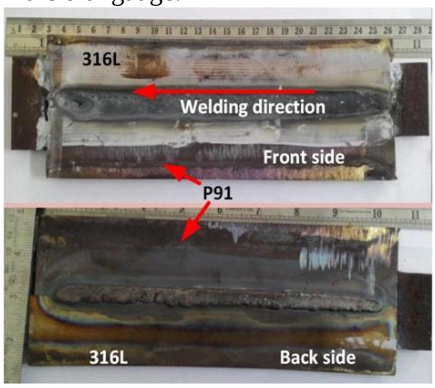

Fig. 2. Image shows the front and back side of the dissimilar metal joint weldments

B. *Macro and micro analysis*

Weld bead geometry Cross-section of the dissimilar weld joint is shown in Fig. 3. It was found, that the weld fusion zone was free from any kind of welding defect such as porosity, crack, undercut, and lack of penetration. The weld width at the top and bottom sections was 10.52 mm and 5.05 mm, respectively. The depth of penetration to width of the weld bead at top surface (D/W) ratio was 0.86. Plate thickness was considered as the maximum depth of penetration because full penetration was achieved. A narrow Heat Affected Zone (HAZ) of width 300 ±100 □m was observed in 316L SS side as compared to P91 steel side HAZ having a width of 6±1 mm. This could be attributed to the higher thermal conductivity of P91 steel as compare to 316L SS. P91 steel HAZ comprised Coarse Grain Heat Affected Zone (CGHAZ), Fine Grain Heat Affected Zone (FGHAZ), and the Intercritical Heat Affected Zone (ICHAZ).

Optical micrograph of the 316L SS - P91steel weldment. Delta ferrite of vermicular shape was observed in the HAZ of the 316L side. SEM micrograph also revealed that the fraction of the delta ferrite was increased on approaching from base metal to the fusion boundary. Lathe martensite and twins were also witnessed in the HAZ of the 316L side. Twins were found near the interface of an unaffected base metal and HAZ, while the lathe martensite was found near fusion boundary. Formation of the delta ferrite in the HAZ of 316L side may be attributed to the high $Cr_{eq}/Ni_{eq}$of 316L steel.

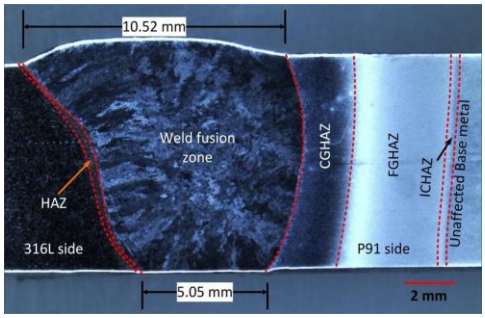

Fig. 3. Optical image shows the macro view of the 316L SS - P91 steel weldment

C. *Mechanical properties*

Hardness was taken across the weld direction covering all the weld zones of the TIG weldment. The obtained hardness profile is shown in Fig. 4. The average hardness calculated in 316L unaffected base metal, 316L HAZ, weld fusion zone, P91 CGHAZ, P91 FGHAZ, and P91 unaffected base metal was 213.4±4.9 HV, 221±3.5 HV, 413±15.7 HV, 450±12.6 HV, 344.1±80.2 HV, and 253.6±4.8 HV respectively. The average hardness of the weld fusion zone (450±12.6 HV) was more than that of the as-received P91 steel (253.6±4.8 HV) and 316L SS (213.4±4.9 HV) base metals. Hardness was found increase toward the P91 steel side. The hardness in the HAZ of AISI 316L was slightly higher than the parent metal due to the agglomeration of delta ferrite stringers. The increase in hardness in the weld fusion zone as compared to base metal could be attributed to the martensitic transformation. Maximum hardness of the weldment was found in the P91 CGHAZ. The high hardness of the P91 CGHAZ as compared to the other weld zones in dissimilar weldment can be attributed to the complete dissolution of the inherent intermetallic phases into the main matrix. Dissolution of the inherent precipitates results in increased Nitrogen (N_2) and Carbon (C) in the solid solution.As this makes CGHAZ stronger and harder as compared to other sections of the weldment such as weld fusion zone.

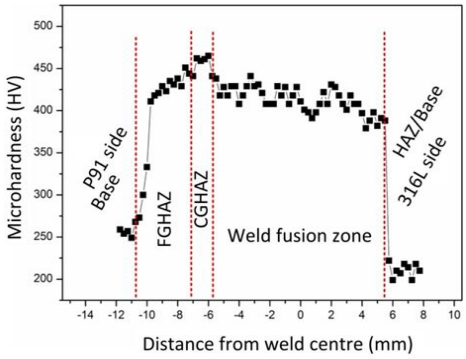

Fig. 4. Micro hardness profile across the dissimilar weldments

Tensile sample before and after. The fractured sample elucidates that the fracture occurred around the fusion boundary in the 316L side. Side view of the tensile fracture sample shows that sample experienced a shear mode of fracture without appreciable necking. The tensile properties such as ultimate tensile strength,

0.2% offset yield strength and the percentage elongation of the A-TIG dissimilar metal weldment observed were 527±2 MPa, 400±5 MPa, and 9±0.4 %, respectively. The tensile studies revealed the presence of a weak section near the 316L fusion boundary. The fracture of the weldment from the adjacent to 316L fusion boundary may be due to the presence of the oxide inclusions near the as discussed in microstructure study. Elongated dimples of different sizes were observed on the fracture surface suggesting the occurrence of the ductile fracture. Cleavage facets were also observed on the fracture surface, besides a number of micro cracks and tear ridges on the fractured surface. Fracture of the 9% Cr and CrMoV dissimilar weld joints from the weld interface was also reported by Qingjun et al. and the same was attributed to the formation of a narrow soft zone due to carbon migration.

Though, transgranular cleavage crack was noticed in the brittle fracture zone of the P91 steel side HAZ fractured surface. More tear ridge in the fracture surface of the P91 steel side HAZ supports the lower Charpy toughness compared to the weld fusion zone and the 316L side HAZ.

4. Conclusion

In the current work, dissimilar weld joint between 316L SS and P91 steel was made by applying newly developed coating

pattern during TIG welding. The weld integrity of the weld joint was investigated through various characterisation techniques such as visual inspection, macrograph analysis of the weld bead, metallurgical study, mechanical testing. Major conclusions drawn from the work are listed below.

- 316L-P91 steel has been successfully welded using single pass A-TIG welding. The weld joint was free from any kind of welding defect such as porosity, crack, undercut, and lack of penetration.
- Gradual increase of hardness in weld fusion zone was observed from 316L side to P91 side. Maximum hardness of 450±12.6 HV was observed in CGHAZ of P91 side, followed by the weld fusion zone hardness (413±15.7 HV).
- Tensile test specimens were failed from the 316L side weld fusion boundary. The UTS of the weldment (527±2 MPa) was lower than that of the parent metals.
- The Charpy impact energy absorbed by the 316L side HAZ, weld fusion zone, and the P91 side HAZ were 60±3 J, 45±4 J, and 18±2 J respectively. The lower Charpy toughness of the P91 steel HAZ was attributed to the presence of untempered martensite with coarse grain structure.

References

[1] C. Pandey, A. Giri, M.M. Mahapatra, Effect of normalizing temperature on microstructural stability and mechanical properties of creep strength enhanced ferritic P91 steel, Mater. Sci. Eng. A. 657 (2016) 173–184.
[2] V. Shankar, M. Valsan, K.B.S. Rao, R. Kannan, S.L. Mannan, S.D. Pathak, Low cycle fatigue behavior and microstructural evolution of modified 9Cr-1Mo ferritic steel, Mater. Sci. Eng. A. 437 (2006) 413–422.
[3] C. Pandey, M.M. Mahapatra, Evolution of phases during tempering of P91 steel at 760 for varying tempering time and their effect on microstructure and mechanical properties, Proc. Inst. Mech. Eng. Part E J. Process Mech. Eng. 664 (2016) 58–74.
[4] S. Paddea, J. a. Francis, a. M. Paradowska, P.J. Bouchard, I. a. Shibli, Residual stress distributions in a P91 steel-pipe girth weld before and after post weld heat treatment, Mater. Sci. Eng. A. 534 (2012) 663–672.
[5] M. Sireesha, V. Shankar, S.K. Albert, S. Sundaresan, Microstructural features of dissimilar welds between 316LN austenitic stainless steel and alloy 800, Mater. Sci. Eng. A. 292 (2000) 74–82.
[6] H.Y. Lee, S.H. Lee, J.B. Kim, J.H. Lee, Creep-fatigue damage for a structure with dissimilar metal welds of modified 9Cr-1Mo steel and 316L stainless steel, Int. J. Fatigue. 29 (2007) 1868–1879.
[7] R.S. Vidyarthy, D.K. Dwivedi, Activating flux tungsten inert gas welding for enhanced weld penetration, J. Manuf. Process. 22 (2016) 211–228.
[8] D.S. Howse, W. Lucas, Investigation into arc constriction by active fluxes for tungsten inert gas welding, Sci. Technol. Weld. Join. 5 (2000) 189–193.
[9] H. Fujii, T. Sato, S. Lu, K. Nogi, Development of an advanced A-TIG (AA-TIG) welding method by control of Marangoni convection, Mater. Sci. Eng. A. 495 (2008) 296–303.
[10] R.S. Vidyarthy, D.K. Dwivedi, Creep behavior of ferritic steel weld joints, in: 7 Int. Conf. Creep, Fatigue Creep-Fatigue Interact., Indira Gandhi Centre for Atomic Research, Kalpakkam, Tamil Nadu, India. January 1922, 2016, Kalpakkam, 2016: pp. 898–903.
[11] K.D. Ramkumar, B.M. Kumar, M.G. Krishnan, S. Dev, A.J. Bhalodi, N. Arivazhagan, et al., Studies on the weldability, microstructure and mechanical properties of activated flux TIG weldments of Inconel 718, Mater. Sci. Eng. A. 639 (2015) 234–244.
[12] R.S. Vidyarthy, D.K. Dwivedi, M. Vasudevan, Influence of M-TIG and A-TIG Welding Process on Microstructure and Mechanical Behavior of 409 Ferritic Stainless Steel, J. Mater. Eng. Perform. 26 (2017) 1391–1403.
[13] R.S. Vidyarthy, D.K. Dwivedi, V. Muthukumaran, Optimization of A-TIG Process Parameters Using Response Surface Methodology, Mater. Manuf. Process. (2017) 10426914.2017.1303154.
[14] T. Sakthivel, M. Vasudevan, K. Laha, P. Parameswaran, K.S.S. Chandravathi, M.D.D. Mathew, et al., Comparison of creep rupture behaviour of type 316L(N) austenitic stainless steel joints welded by TIG and activated TIG welding processes, Mater. Sci. Eng. A. 528 (2011) 6971–6980.
[15] B. Arivazhagan, M. Vasudevan, A comparative study on the effect of GTAW processes on the microstructure and mechanical properties of P91 steel weld joints, J. Manuf. Process. 16 (2014) 305–311.
[16] P.S. Wei, F.K. Chung, Unsteady Marangoni Flow in a Molten Pool When Welding Dissimilar Metals, Metall. Mater. Trans. B. 31B (2000) 1387–1403.
[17] P.S. Wei, Y.K. Kuo, J.S. Ku, Fusion Zone Shapes in Electron-Beam Welding Dissimilar Metals, J. Heat Transfer. 122 (2000) 626.
[18] H.K. Cheng, L.T. Yao, P.C. Chang, A Study of the Performance of Dissimilar A-TIG Welds, Adv. Mater. Res. 530 (2012) 74–79.
[19] P. Wang, S.P. Lu, N.M. Xiao, D.Z. Li, Y.Y. Li, Effect of delta ferrite on impact properties of low carbon 13Cr–4Ni martensitic stainless steel, Mater. Sci. Eng. A. 527 (2010) 3210–3216.
[20] K. Devendranath Ramkumar, A. Bajpai, S. Raghuvanshi, A. Singh, A. Chandrasekhar, M. Arivarasu, et al., Investigations on structure–property relationships of activated flux TIG weldments of super-duplex/austenitic stainless steels, Mater. Sci. Eng. A. 638 (2015) 60–68.
[21] K.-H. Tseng, Study on surface appearance, geometry size, and delta-ferrite content of ZrO2-aided TIG welding of AISI 316LN stainless steel, Int. J. Adv. Manuf. Technol. (2016) 1–8.
[22] M. Pouranvari, M. Khorramifar, S.P.H. Marashi, Ferritic–austenitic stainless steels dissimilar resistance spot welds: metallurgical and failure characteristics, Sci. Technol. Weld. Join. 21 (2016) 438–445.
[23] H. Zheng, X. Ye, L. Jiang, B. Wang, Z. Liu, G. Wang, Study on microstructure of low carbon 12% chromium stainless steel in high temperature heat-affected zone, Mater. Des. 31 (2010) 4836–4841.
[24] C. Pandey, M.M. Mahapatra, Effect of Groove Design and Post-Weld Heat Treatment on Microstructure and Mechanical Properties of P91 Steel Weld, J. Mater. Eng. Perform. 25 (2016) 2761–2775.
[25] Q. Wu, F. Lu, H. Cui, X. Liu, P. Wang, Y. Gao, Soft zone formation by carbon migration and its effect on the high-cycle fatigue in 9% Cr-CrMoV dissimilar welded joint, Mater. Lett. 141 (2015) 242–244.
[26] J.R. Scully, D.W. Taylor, Electrochemical Methods of Corrosion Testing, in: ASM Handbook, Vol. 13, 9th Ed., 9th Edition, ASM, 1987: p. 458.
[27] P.E. Manning, D.J. Duquette, W.F. Savage, Technical Note: The Effect of Retained Ferrite on Localized Corrosion in Duplex 304L Stainless Steel, Weld. Res. Suppl. (1980) 260–262.